A Comparison of Error Indicators for Multilevel Visualization on Nested Grids

Thomas Gerstner, Martin Rumpf, and Ulrich Weikard

Department for Applied Mathematics, University of Bonn, Germany

Abstract. Multiresolution visualization methods have recently become an indispensable ingredient of real time interactive post processing. Here local error indicators serve as criteria where to refine the data representation on the physical domain. In this article we give an overview on different types of error measurement on nested grids and compare them for selected applications in 2D as well as in 3D. Furthermore, it is pointed out that a certain saturation of the considered error indicator plays an important role in multilevel visualization and can be reused for the evaluation of data bounds in hierarchical searching or for a multilevel backface culling of isosurfaces.

1 Introduction

A variety of multiresolution visualization methods has been designed to serve as tools for interactive visualization of large data sets [3, 9, 12, 20]. Here the local resolution of the generated visual objects, such as 2D graphs, or isosurfaces and color shaded slices in 3D, depends on error indicators which measure the error due to a locally coarser approximation of the data.

Different approaches have been presented to solve the outstanding continuity problem, i.e. to avoid cracks in adaptive isosurfaces. In the Delaunay approach by Cignoni et al. [4] and in the nested mesh method by Grosso et al. [10] the successive remeshing during the refinement guarantees continuity. Alternatively, Shekhar et al. [21] rule out hanging nodes by inserting additional points on faces with a transition from finer to coarser elements due to an adaptive stopping criterion.

We apply the method of adaptive projection on nested grids, which has been described in earlier publications. For the general concept we refer to [18]. Implementational aspects are especially described in [17]. The core of our approach is identical to the method of Zhou et al. [24]. In 3D it can be regarded as a generalization of the techniques presented by Livnat et al. [15] and in [8].

In this paper we give a detailed comparison of error indicators and the performance of corresponding multilevel methods. Here we do not focus on the methodology itself but on the indicators, their effect on cost reduction, and their relation to the actual error in a corresponding norm. Therefore, especially to simplify the exposition, we confine ourselves to simplicial grids generated by bisection, which are well known from adaptive numerical methods [1, 19]. In explicit, we deal with the recursive bisection of [13, 16].

Let us point out that there are other, more general approaches especially for surfaces by De–Floriani et al. [6] and Hamann and Chen [11] which also apply to non nested grid hierarchies, but with a different focus concerning the field of applicability.

2 A general multilevel algorithm on nested grids

We confine ourselves here to hierarchical simplicial grids which carry a piecewise linear data function. Let us consider a family of nested, conforming, simplicial meshes $\{\mathcal{T}^l\}_{0\le l\le l_{\max}}$ in two or three dimensions. We denote by $h(T)$, $h(e)$ the diameter, respectively the length of an edge e of a simplex $T \in \mathcal{T}^l$. Furthermore, $\mathcal{N}(T)$, $\mathcal{N}(\mathcal{T}^l)$ denote nodal sets of single simplices, respectively entire triangulations.

The simplices, triangles in 2D, respectively tetrahedra in 3D are assumed to be refined by recursive bisection. For a simplex T, the midpoint of a predestined edge $e_{\text{ref}}(T)$ is thereby picked up as a new node $x_{\text{ref}}(T)$, and the simplex is cut at the edge, respectively face, $F_{\text{ref}}(T)$ spanned by $x_{\text{ref}}(T)$ and the nodes of T, which are not endpoints of the refinement edge $e_{\text{ref}}(T)$, into two child simplices $\mathcal{C}(T) = \{T^1_{\mathcal{C}}, T^2_{\mathcal{C}}\}$. A simple alternating scheme for the refinement edge e_{ref} [1, 13] guarantees the conformity of the resulting grids. Finally, let U^l denote the piecewise linear function on $\mathcal{T}^l$ uniquely described by the data values on the corresponding nodes.

The multilevel algorithm is based on a depth first traversal of the grid hierarchy. On every simplex we check for a stopping criterion. If it is true we stop and visualize locally. Otherwise, we recursively proceed on the child set $\mathcal{C}(T)$.

If we stop on a specific simplex T and refine another simplex $\tilde{T}$ which shares the refinement edge with T, i.e. $e_{\text{ref}}(T) = e_{\text{ref}}(\tilde{T})$, an inconsistency occurs at the hanging node x_{ref}. This leads to jumps in the color intensity or cracks in the isosurface. In the case of general nested grids we can apply adaptive projection operators to ensure consistency [18]. Here, we simply have to ensure that, whenever a simplex is refined, all the simplices sharing its refinement edge – in 2D only the one triangle opposite to T at the edge $e_{\text{ref}}(T)$ – are refined as well.

This can be achieved by defining error indicators $\eta(x)$ on the grid nodes and choosing $\eta(x_{\text{ref}}(T)) < \varepsilon$ as stopping criterion on a simplex for some user prescribed threshold value ε. Since all nodes, except those on the coarsest level, are refinement nodes $x_{\text{ref}}(T)$ on a refinement edge $e_{\text{ref}}(T)$, the indicator value $\eta(x)$ measures the error on those simplices sharing the edge. Therefore, the recursive traversal would stop not only on T but – if visited – on all other simplices sharing the refinement edge if their common stopping criterion is true.

However, for an arbitrary error indicator it might still occur that, although $\eta(x_{\text{ref}}(T)) < \varepsilon$, $\eta(x_{\text{ref}}(\hat{T})) \ge \varepsilon$ on some descendant $\hat{T}$ whose refinement node $x_{\text{ref}}(\hat{T})$ is located on the boundary of T. The adjacent tetrahedron will possibly be visited and then refined, whereas on T the stopping criterion already holds. To avoid this we assume the following saturation condition on the error indicator (for a generalization compare [18]):

Saturation Condition:
$\eta(x_{ref}(T)) > \eta(x_{ref}(T_{\mathcal{C}}))$ *for all* $T \in \mathcal{T}^l$ *with* $l < l_{max}$ *and* $T_{\mathcal{C}} \in \mathcal{C}(T)$.

An error indicator η is called admissible, if it fulfills the saturation condition. Otherwise, it can easily be adjusted in a preroll step (cf. section 3). The adaptive algorithm can be sketched in pseudo code as follows

```
Inspect(T) {
    if SimplexIsOfInterest(T)
        if C(T) ≠ ∅ ∧ η(x_ref(T)) ≥ ε
            { Inspect(T_C^1); Inspect(T_C^2); }
        else Extract(T);
}
```

where the function *SimplexIsOfInterest()* checks whether the simplex is a candidate for some local rendering or not. For example, in 3D slicing the cutting plane has to intersect the simplex T. In multilevel isosurface extraction this function checks whether the isosurface intersects the current simplex. At the end of the next section we show how this function can be implemented efficiently.

3 An overview of error measurement

In this section we will discuss several principle techniques of error measurement. The starting point will be some actual local error measure on the grid hierarchy. The local resolution and the visual impression of the numerical data is closely related to the specific type of error measurement applied in the adaptive traversal of the tree structure.

Choices for the error metric

Let $\eta^*(x)$ be a measure on nodes x, which weights the effect of stopping for some local rendering already on a simplex T with $x = x_{ref}(T)$ instead of traversing the locally finest grid level. Furthermore, let us denote by $S(x)$ the support of the piecewise linear base function corresponding to the node x. Then, given a fine grid data function U and a coarse grid function U^l on level l with $T \in \mathcal{T}^l$, we assume $\eta^*(x)$ to be the distance between U and U^l measured locally on $S(x)$ by some metric $d_{S(x)}$, i.e.

$$\eta^*(x) = d_{S(x)}(U, U^l)$$

Let us consider several widely used metrics:

- We can choose some local norm of the difference functions such as

  $$\eta^*(x) := \|U - U^l\|_{p,S(x)},$$

  where $\|\cdot\|_{p,S(x)}$ is the usual L^p norm for $p \in [1, \infty]$ restricted to the domain $S(x)$. Due to Hölder's inequality the error indicators obviously become sharper for increasing values of p.

– Instead of function values we can consider derivatives and define

$$\eta^*(x) := \|\nabla U - \nabla U^l\|_{p,S(x)} .$$

In general the resulting error measurement is sharper then the one based on function values. By some worst case analysis based on inverse estimates we obtain the estimate

$$\|\nabla U - \nabla U^l\|_{p,S(x)} \leq C\, h_{\min}^{-1} \|U - U^l\|_{p,S(x)}$$

where $h_{\min} := \min_{T \in \mathcal{T}_{l-1},\, T \subset S(x)} h(T)$. This estimate is asymptotically sharp on fine grid levels for a function U, which is the interpolation of some smooth function. Frequently, the norm of the gradient is taken as an error indicator. This is questionable, because rendering is "linearly exact" and therefore refinement in areas of uniformly large gradient norms does not improve the graphical representation.

– Third – a smooth graphical representation in mind – we may be interested in measuring the geometric smoothness of the approximation independently of the true function values. A possible measure is a discrete curvature quantity. For surfaces this should be related to the absolute curvature $\kappa = \sqrt{\kappa_1^2 + \kappa_2^2}$ where the κ_i are the principle curvature terms. As clearly indicated in the case of minimal surfaces with vanishing mean curvature or cylinders with vanishing Gaussian curvature, mean or Gaussian curvature discretization does not make sense in terms of general error control.

– A fourth choice of a suitable measure is closely related to geometric shapes [14]. In our simple case of a scalar function U a suitable approach is to compare the graphs of U, respectively U^l on $S(x)$. If $\mathrm{dist}(\cdot,\cdot)$ is a geometric distance metric on graphs, we are lead to $\eta^*(x) := \mathrm{dist}(graph(U), graph(U^l))$. For flat graphs this error indicator only slightly differs from measuring the difference of the function values.

Furthermore, the viewing direction and distance may enter the error metric [15], or the error measurement may depend on the distance to a specific region of interest [2, 5, 18]. We will here restrict ourselves to the basic error norms and discrete curvature measurement.

Hierarchical error measurement

Usually, an error measurement which locally compares coarse grid functions with the functions on the finest grid is expensive to evaluate even in a preprocessing step. We will apply an often used simplification, which only compares data on the current grid level to data on the next finer grid level. We will denote the corresponding one level look ahead error indicator by $\eta(x)$. However, the saturation condition as a minimum precondition to guarantee continuity of the adaptive projection may fail for η.

– **Hierarchical offset error indicators:** In analogy to the norm of the difference function we can consider the hierarchical offset function U_δ defined on a tetrahedon as

$$U_\delta|_T = U_l|_T - U_{l-1}|_T$$

The values of U_δ on $\mathcal{N}^l \setminus \mathcal{N}^{l-1}$ are related to the original data values by the following recursive formula

$$U(x_{\text{ref}}(T)) = \frac{U(x_1) + U(x_2)}{2} + U_\delta(x_{\text{ref}}(T))$$

where x_1 and x_2 are the end points of the edge corresponding to $x_{\text{ref}}(T)$ on a simplex T. For smooth data, i.e. $U(x) = u(x)$ for all nodes x with $u \in C^2$, $|U_\delta(x_{\text{ref}}(T))| = O(h(T)^2)$, which implies the saturation condition holds asymptotically on grids $\mathcal{T}^l$ for l sufficiently large. Let us emphasize that the handling of the U_δ–values would therefore allow an economical δ–compression of the data. The original values can easily be retrieved during the recursive tree traversal. Now, we define the hierarchical L^∞ error indicator

$$\eta_\infty(x) := |U_\delta(x)| \,.$$

Instead of the L^∞ norm we can analogously consider different integral norms applied to the difference function which corresponds to a new node. Using lumped mass integration we obtain

$$\eta_p(x) = \frac{1}{3}\left(\sum_{T\,,\,x\in\mathcal{N}(T)} |T|\right)^{\frac{1}{p}} |U_\delta(x)|$$

for $1 \le p < \infty$. Decreasing p leads to an earlier stopping of the tree traversal on simplices of small size.

– **Gradient type error indicator:** Instead of measuring the one level error with respect to function values, we can consider the error of the function gradient. We thus define

$$\eta_{1,p}(x) := \begin{cases} \left(\displaystyle\sum_{T\,,\,x\in\mathcal{N}(T)} |T|\right)^{\frac{1}{p}} \|\nabla U_\delta|_T\| & \text{for} \quad 1 \le p < \infty, \\ \displaystyle\max_{T\,,\,x\in\mathcal{N}(T)} \|\nabla U_\delta|_T\| & \text{for} \quad p = \infty. \end{cases}$$

The evaluation of these error indicators takes some effort in the precomputing step. If we replace simplices by simplex refinement edges without modifying the scaling we gain at least for $p = \infty$

$$\eta_{N,e} := \frac{2\,|U_\delta(x_{\text{ref}}(T))|}{h(e_{\text{ref}}(T))}.$$

– **Discrete curvature type indicators:** With a focus on an isosurface's geometric shape, we will now consider some kind of curvature estimation. We ask for a discrete curvature quantity which locally measures the quality of the data approximation from the perspective of the visual appearance [18]. In isosurface images consisting of linear patches we can easily recognize folds at surface edges. In each tetrahedron the data gradient ∇U^l is always perpendicular to an isosurface. Therefore, at any face F the normal component of the jump of the normalized gradient, denoted by $[\frac{\nabla U^l}{|\nabla U^l|}]_F$, locally measures the fold in the data function. Here the jump operator $[\cdot]_F$ is defined as the difference of the argument on both sides of the face. This jump obviously serves as a well–founded graphical error criterion and motivates the definition

$$\eta_N(x_{\text{ref}}(T)) := \left[\frac{\nabla U^l}{|\nabla U^l|}\right]_{F_{\text{ref}}(T)} .$$

We can apply the simplification of the previous indicator here as well and denote the resulting error indicator by $\eta_{N,e}$.

Ensuring the saturation condition

As pointed out above, the hierarchical error indicators do not fulfill the saturation condition. We can overcome this drawback by defining a modified error indicator $\bar{\eta}$, which is defined as the minimal saturated error indicator larger or equal to η. This definition is constructive in the sense that in a bottom up, breadth first traversal of the grid, we can blow up these error indicator values. In pseudo code this blow up mechanism looks as follows:

```
for (l = l_max − 1 ; l ≥ 0 ; l−− )
    for all T ∈ T^l and x = x_ref(T)
        η̄(x) = max{ max_{T_C ∈ C(T)} η̄(x_ref(T_C)), η(x) };
```

Let us emphasize that a depth first traversal of the hierarchy in the adjustment procedure would not be sufficient. If the error indicators are adjusted in this way the continuity problems are solved automatically.

Recursive blowup

Alternatively, we can ensure saturation of an indicator η by recursively defining:

$$\eta^+(x) = \eta(x) + \max_{T_C \in \mathcal{C}(T)} \eta^+(x_{\text{ref}}(T)) \qquad \text{for } x = x_{\text{ref}}(T).$$

On the finest grid level, where $C(T) = \emptyset$, we simply set $\eta^+(x) = \eta(x)$. The different error measures are obviously related to each other by $\eta \leq \bar{\eta} \leq \eta^+$.

Furthermore, we obtain $\eta^*_\infty \leq \eta^+_\infty$ and $\eta^*_{1,\infty} \leq \eta^+_{1,\infty}$ due to the triangle inequality. The indicator η^+, although the largest one derived from the original indicator η^*, and thus the weakest, can have other desirable properties. For instance, an easy computation of min/max-values for isosurface extraction or criteria for multilevel backface culling are possible, which is demonstrated next.

On the one hand, we are able to compute a bound $\beta_0(T)$ for second order offset terms of the data function on a simplex $T \in \mathcal{T}^l$, i.e. the difference of the true function and its linear approximation. This can be applied in the implementation of the *SimplexIsOfInterest()*-function. We obtain

$$\min_{x \in T} U^l - \beta_0(T) \leq U \leq \max_{x \in T} U^l + \beta_0(T)\,.$$

The *SimplexIsOfInterest()* routine corresponding to the extraction of an isosurface for the isovalue c can be written in pseudo code:

```
SimplexIsOfInterest(T) {
    if min_{x∈N(T)} U(x) − β0(T) ≤ c ≤ max_{x∈N(T)} U(x) + β0(T)
        return true;
    else
        return false;
}
```

In the hierarchical offset case and for the choice η^+_∞ we can define

$$\beta_0(T) = \begin{cases} \frac{1}{2}\eta^+_\infty(x_{\text{ref}}(T)), & \text{for hierarchical offset indicators} \\ h(T)\eta^+_{1,\infty}(x_{\text{ref}}(T)), & \text{for gradient type indicators} \end{cases}$$

In both cases, the expensive storing of min/max–values as discussed in [23] can be avoided.

On the other hand, we may check – based on coarse grid simplices – whether all polygons extracted by the algorithm will be backfaces. Let $N^l = \frac{\nabla U^l}{\|\nabla U^l\|}$ denote the normal of some triangle of the final isosurface triangulation on the simplex $T \in \mathcal{T}^l$, and V the viewing vector from the object to the eye (we confine ourselves here to parallel projection). If $N^l \cdot V \geq 0$, the triangle is faced towards the viewer. Otherwise it does not need to be drawn. We obtain a significant acceleration of our isosurface algorithm, if on a much coarser grid level we recognize simplices containing only isosurface triangles which are faced away from the viewer so that we are already able to stop the local traversal at this level. If $\beta_N(T)$ is a bound of the modification of N^l in $T \in \mathcal{T}^l$, we obtain the multilevel backface test

$$N^l \cdot V + \beta_N(T) \leq 0, \qquad \text{with } \beta_N(T) := {\eta^+}_N(x_{\text{ref}}(T))$$

for the discrete curvature type error indicator ${\eta^+}_N$.

Skipping the normalization and considering instead a bound $\beta_1(T)$ which measures the possible offset in $\|\nabla U\|$, we alternatively obtain the rejection criterion

$$\nabla U^l \cdot V + \beta_1(T) \leq 0, \qquad \text{with } \beta_1(x) = \eta^+_{1,\infty}(x_{\text{ref}}(T))\,.$$

It can easily be seen that, on average, while arbitrarily rotating the object, we save up to one half of the computing time for an isosurface.

4 A quantitative comparison

Up to now we have analyzed qualitative aspects of different error indicators. In what follows, let us focus on a detailed quantitative discussion. Therefore, we study certain test problems in 2D as well as in 3D.

Test data sets

In 2D we pick up different examples from different classes of data sets. On the one hand, we choose a typical measurement data set, which represents a geographical map, originally sampled on a 257^2 regular grid, which we afterwards cover with a hierarchical triangular grid (see Appendix). It consists of regions with a significant roughness and other areas which are almost planar.

On the other hand, we apply multilevel visualization to a typical numerical data set already computed on a triangular grid hierarchy. It is characterized by smooth, less steep areas which alternate with thin transition zones where the data function is rather steep. Nevertheless, the frequencies are, on average, much more damped in the latter data set, and the numerical data set is much smoother than the geographical map. Here we consider a timestep of a Cahn-Hilliard simulation on the same 257^2 regular grid (see Appendix). It represents the density of an alloy after quenching (rapidly cooling), which leads to phase separation [7, 22].

In the 3D case we consider isosurface extraction and color slicing (see Appendix). Here the well known 129^3 bucky ball data set serves as an example. Like the Cahn-Hilliard data set it contains smooth areas in the interior of the molecule and steep areas in the vicinity of the carbon atoms.

Measures of cost, quality and efficiency

The cost of the visualization method is mainly controlled by the number of visited grid cells in the recursive traversal. We suppose that a suitable graphics hardware guarantees a fast processing and final rendering of graphic primitives on the adaptively finest grid levels, so that the CPU and not the graphics hardware is the bottleneck. Since error indicators come along with different ranges of indicator values on the grid nodes, we ensure comparability by normalizing the maximal indicator value to 1.

An alternative measure of the cost would be the number of rendered primitives. Not surprisingly both measures are closely related and therefore it does not really matter which one we choose. In our experiments there is at most a ratio of logarithmic size with respect to the maximal depth of the grid hierarchy. The following results are based on the visited-cell-count cost measure.

The crucial measure of the quality of an adaptive projection in visualization is the visual impression of the rendered image. However, this is impossible to quantify. So in order to get a comparable notion of the quality we chose the reciprocal of the corresponding global norm of the difference between the adaptively extracted function and the function on the finest grid. In this context the

efficiency E of an error indicator is the quotient of quality and cost and would thus be

$$E_\eta(U,\varepsilon) = \frac{1}{k \cdot \|P_\eta U - U\|}$$

where k is the number of visited cells used for the adaptive projection $P_\eta U$.

Results

Fig. 1 and 2 compare results obtained for the different classes of error indicators. The scaling on the y axes is logarithmic. For the geographical data the different characteristics of the hierarchical offset error indicators compared to the error indicators based on derivatives are striking.

The smoother numerical data show a similar behaviour. Not surprisingly, the graphs for $\bar{\eta}_N$ and $\bar{\eta}_{N,e}$ are especially for the geographical data set nearly the same. Therefore, the simplification incorporated in $\bar{\eta}_{N,e}$ seems to be admissible and as $\bar{\eta}_{N,e}$ is easier to calculate, it is more favourable for practicable purposes than $\bar{\eta}_N$. As also can be expected, the indicators $\bar{\eta}_1$ and $\bar{\eta}_2$ are – in comparison to $\bar{\eta}_\infty$ – rather similar.

The efficiency of these indicators is depicted in Fig. 3. It becomes clear that $\bar{\eta}_\infty$ is less efficient than $\bar{\eta}_1$ and $\bar{\eta}_2$. In the case of the geographical data set and also for not too high threshold values in the case of the numerical data, the qualities of the three error indicators differ only slightly. So the main reason for the low efficiency of $\bar{\eta}_\infty$ is that even for high threshold values a large number of cells is visited. In the 3D-case the results are similar.

Finally, we compare the different methods for ensuring the saturation condition in case of the η_∞-indicator. In our experiments the differences in smoothness between the geographical and the numerical data are clearly visible in the characteristic if $\bar{\eta}_\infty$ is used. However, these differences are lost for η_∞^+. This is also true for other indicators as for example η_2^+ compared to $\bar{\eta}_2$. Hence, an application of an η^+-type saturated indicator is only reasonable if the advantages concerning min/max-bounds or backface culling are exploited.

Visual Impression

We also want to show that for reasonable threshold values the visual impression of the original and adaptively projected images are rather close (see Appendix). For the geographical map, the adaptive image consists of 13666 patches whereas the original image has a size roughly ten times larger (131072 patches). Additionally, we show extracted isosurfaces of the bucky ball data set with 128709 and 590018 triangles, respectively (see Appendix). In all these figures we used the $\bar{\eta}_\infty$ error indicator.

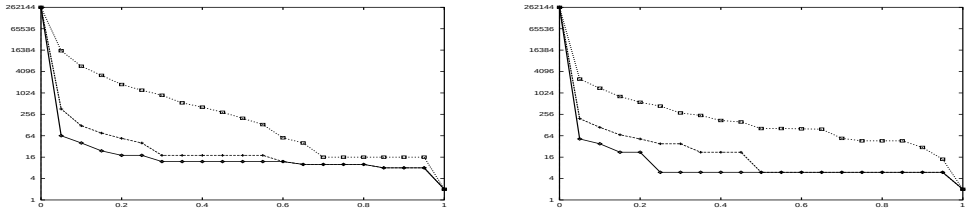

(a) geographical data (b) numerical data

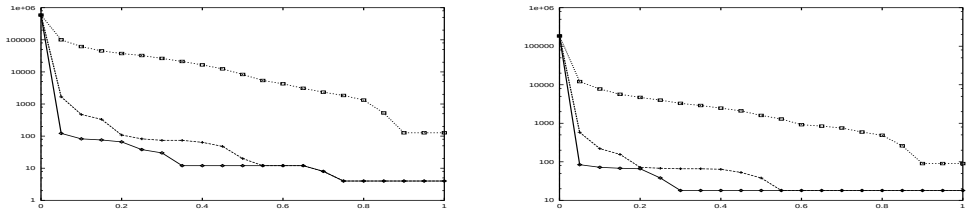

(c) isosurface (d) slice

Fig. 1. Error indicators $\bar{\eta}_1$ (dashed), $\bar{\eta}_2$ (solid) and $\bar{\eta}_\infty$ (dotted) based on the different local L^1, L^2 and L^∞ norms of the hierarchical offset are compared, concerning the count of visited simplices for varying threshold values.

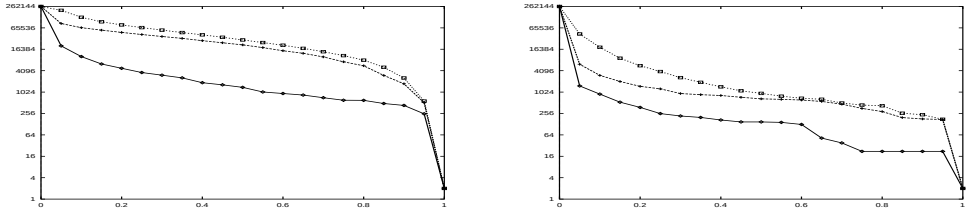

(a) geographical data (b) numerical data

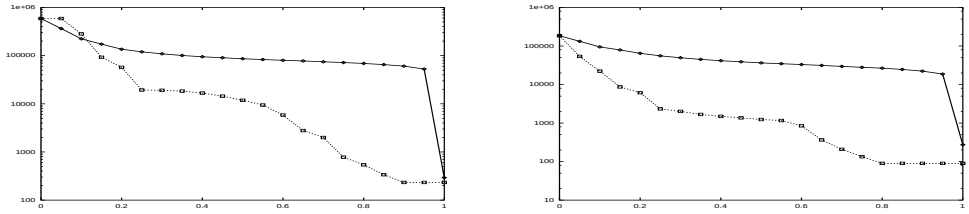

(c) isosurface (d) slice

Fig. 2. The visited cell count is compared for the error indicators $\bar{\eta}_{1,\infty}$(solid), $\bar{\eta}_N$(dotted), and $\bar{\eta}_{N,e}$(dashed, only 2D) respectively.

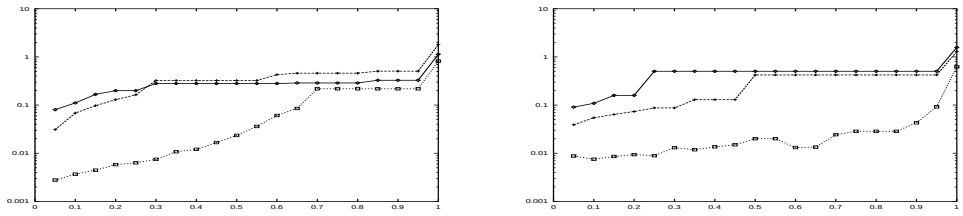

(a) geographical data (b) numerical data

Fig. 3. Efficiency as function of threshold value for local $\bar{\eta}_\infty$-error (dotted), $\bar{\eta}_1$-error (solid) and local $\bar{\eta}_2$-error (dashed)

5 Concluding remarks

In this paper we have considered several error indicators which are used in multiresolutional visualization and compared their quantitative as well as their qualitative properties. We have specifically looked at local norms of difference functions, differences of gradients and discrete curvature measures. We have employed the saturation condition as an important prerequisite for interactive visualization since it solves the continuity problem.

We have shown how this condition can be fulfilled by a blowup of η. We have thereby defined the minimal saturated hierarchical error indicator $\bar{\eta}$, which indeed gives very good results concerning triangle count vs. global error.

On the other hand, by a slight alteration of the blowup mechanism, we have defined the error indicators η^+, which have a slightly worse efficiency but other desirable properties. For instance, based on the error indicator data bounds on simplices can be computed which then serve as stopping criteria for multiresolutional isosurface extraction. We have also shown how gradient type error indicators allow multilevel backface culling. In a series of numerical experiments on application data the different error indicators have been compared and their mutual advantages have been outlined.

References

1. E. Bänsch. Local mesh refinement in 2 and 3 dimensions. *IMPACT of Computing in Science and Engineering*, 3:181–191, 1991.
2. E. Bier, M. Stone, K. Pier, W. Buxton, and T. DeRose. Toolglass and magic lenses: the see–through interface. In *Proceedings of SIGGRAPH '93 (Anaheim, CA, August 1-6). In Computer Graphics Proceedings, Annual Conference series, ACM SIGGRAPH*, pages 73–80, 1993.
3. A. Certain, J. Popović, T. DeRose, T. Duchamp, D. Salesin, and W. Stuetzle. Interactive multiresolution surface viewing. In *SIGGRAPH 96 Conference Proceedings*, pages 91–98, 1996.

4. P. Cignoni, L. De Floriani, C. Montoni, E. Puppo, and R. Scopigno. Multiresolution modeling and visualization of volume data based on simplicial complexes. In *1994 Symposium on Volume Visualization*, pages 19–26, 1994.
5. P. Cignoni, C. Montani, and R. Scopigno. MagicSphere: an insight tool for 3D data visualization. *Computer Graphics Forum*, 13(3):317–328, 1994.
6. L. De Floriani, P. Magillo, and E. Puppo. Building and traversing a surface at variable resolution. In *Proceedings IEEE Visualization 97*, October 1997.
7. C. Elliot. The cahn-hilliard model for the kinetics of phase separation. *Num. Math.*, 1988.
8. T. Gerstner. Adaptive hierarchical methods for landscape representation and analysis. In S. Hergarten and H.-J. Neugebauer, editors, *Lecture Notes in Earth Sciences 78*. Springer, 1998.
9. M. H. Gross and R. G. Staadt. Fast multiresolution surface meshing. In *Proceedings Visualization*, pages 135–142, 1995.
10. R. Grosso, C. Luerig, and T. Ertl. The multilevel finite element method for adaptive mesh optimization and visualization of volume data. In *Proceedings Visualization*, 1997.
11. B. Hamann and J. Chen. Data point selection for piecewise trilinear approximation. *Computer Aided Geometric Design*, 11, 1994.
12. H. Hoppe. Progressive meshes. In *SIGGRAPH 96 Conference Proc.*, pages 99–108, 1996.
13. J. Maubach. Local bisection refinement for n-simplicial grids generated by reflection. *SIAM J. Sci. Comput.*, 16:210–227, 1995.
14. R. Klein, G. Liebich, and W. Straßer. Mesh reduction with error control. In *Proceedings Visualization*, 1996.
15. Y. Livnat, H. W. Shen, and C. R. Johnson. A near optimal isosurface extraction algorithm using the span space. *Transaction on Visualization and Computer Graphics*, 2(1):73–83, 1996.
16. W. F. Mitchell. A comparison of adaptive refinement techniques for elliptic problems. *ACM Trans. on Math. Software*, 15(4):326–347, 1989.
17. R. Neubauer, M. Ohlberger, M. Rumpf, and R. Schwörer. Efficient visualization of large scale data on hierarchical meshes. In W. Lefer and M. Grave, editors, *Visualization in Scientific Computing '97*. Springer, 1997.
18. M. Ohlberger and M. Rumpf. Adaptive projection methods in multiresolutional scientific visualization. *IEEE Transactions on Visualization and Computer Graphics, Vol 4 (4)*, 1998.
19. M. C. Rivara. Algorithms for refining triangular grids suitable for adaptive and multigrid techniques. *Internat. J. Numer. Methods Engrg.*, 20:745–756, 1984.
20. W. J. Schroeder, J. A. Zarge, and W. A. Lorensen. Decimation of triangle meshes. In *Computer Graphics (SIGGRAPH '92 Proceedings)*, volume 26, pages 65–70, 1992.
21. R. Shekhar, E. Fayyad, R. Yagel, and J. F. Cornhill. Octree-based decimation of marching cubes surfaces. In *Proceedings Visualization*. IEEE, 1996.
22. U. Weikard. Finite-Element-Methoden für die Cahn-Hilliard-Gleichung unter Einbeziehung elastischer Materialeigneschaften. Diplomarbeit, 1998.
23. J. P. Wilhelms and A. Van Gelder. Octrees for faster isosurface generation. In *Computer Graphics (San Diego Workshop on Volume Vis.)*, volume 24, 5, pages 57–62, 1990.
24. Y. Zhou, B. Chen, and A. Kaufman. Multiresolution tetrahedral framework for visualizing volume data. In *IEEE Visualization '97 Proceedings*. IEEE Press, 1997.

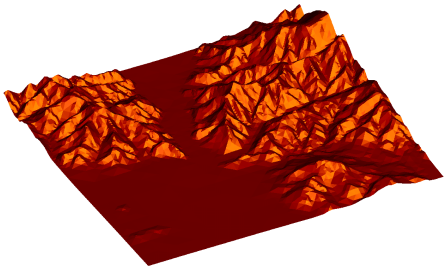

(a) Adaptive projection of the geographical map

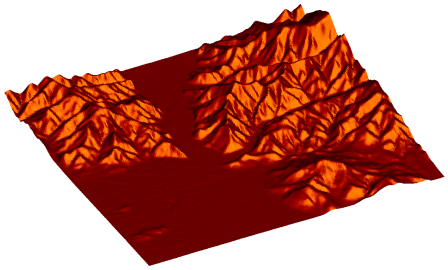

(b) Original data

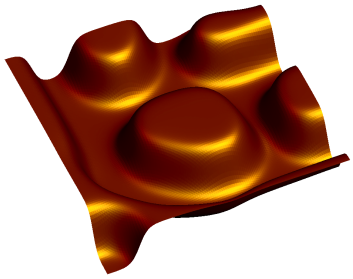

(c) Timestep of Cahn-Hilliard Equation

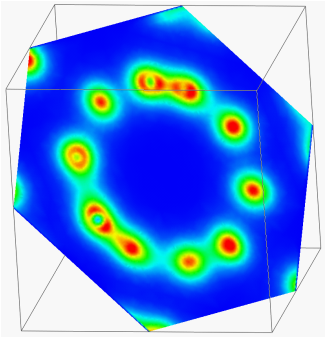

(d) Color shaded slice of the bucky ball

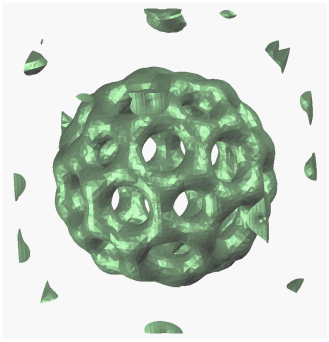

(e) Adaptive projection of the isosurface

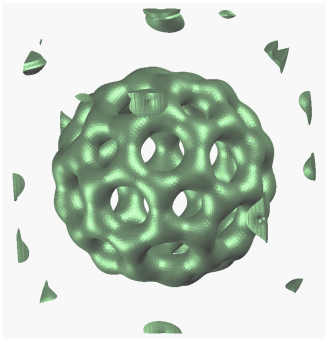

(f) Original data

Fig. 4. Above the graph of a geographic height field, its adaptive projection and a timestep of the Cahn-Hilliard-Equation are shown. Of the bucky ball data set we show a color shaded diagonal slice, an adaptive projection and a full resolution isosurface.